Adsorptive removal of heavy metals from aqueous solution by graphene oxide modified membranes

N.P. Khumalo[1], S.D. Mhlanga[1], A.T. Kuvarega[1], G. D. Vilakati[2], B.B. Mamba[1], D.S. Dlamini[1]*

[1] *Nanotechnology and Water Sustainability (NanoWS) Research Unit, College of Science, Engineering and Technology, University of South Africa, Florida Science Campus, South Africa.*

[2] *Department of Chemistry, University of Swaziland, Private Bag 4, Kwaluseni, M201, Swaziland*

Abstract— Heavy metals are a concern in the environment as they accumulate and are non-biodegradable and thus bio-toxic. Many technologies have been employed for the removal of heavy metals in the environment. However, adsorption process is arguably the most promising and effective fundamental approach for the removal of heavy metals in wastewater treatment processes. This research is based on modification of PSf polymer membranes with GO for applications as adsorbents for metal ion removal from water. Incorporation of GO in PSf improved the hydrophilicity of the membranes. SEM analysis showed porous membrane surfaces with uneven pore distribution. Pb^{2+} adsorption (>80%) was pH dependent and followed the Langmuir adsorption isotherm. It was demonstrated that the hybrid membranes can be used for removal of metal ions from wastewater.

Index Terms— Heavy metals, graphene oxide, metals oxide-graphene oxide nanohybrids, membrane adsorbents.

1 INTRODUCTION

INDUSTRIAL waste accompanied by the disposal of heavy metals has triggered a global campaign for heavy metals removal in water. The major concern is the ability of heavy metals to accumulate in the environment, as well as their non-biodegradability and then bio-toxicity [1]. Unlike most organic pollutants, heavy metals are not biodegradable and cannot be metabolized or decomposed [2] [3] [3] [4]. Heavy metals can enter the food chain, posing adverse health risks, which are chronic in the long term [6], [7]. These health risks include pulmonary fibrosis, lung cancer as a result of chromium inhalation, nerve and skin damage as a result of exposure to arsenic, lead exposure may result in central nervous system, kidney and liver failure [8], [9]. A number of available scientific literature seeks to imperatively address and solve the challenge of heavy metals removal in portable and wastewater [10]. Technologies such as chemical precipitation, electrochemical removal, ion exchange, solvent extraction, nanofiltration, reverse osmosis and adsorption have been employed for the removal of heavy metals [11]. However, the most suitable processes for heavy metal removal depends on parameters such as, pH, heavy metal concentration, removal efficiency, effect of co-existing pollutants, environmental impacts and the process costs.

Adsorption process is arguably the most promising and effective fundamental approach for the removal of heavy metals during water and wastewater treatment processes. This is due to the flexibility in design and operation, simplicity, convenience and efficiency of the adsorption process [12]. Nanotechnology offers more effective and structurally precise adsorbents for the adsorptive removal of heavy metals. Examples include agricultural by products [13] zeolites [14], activated carbon [15][16], graphene oxide based nanoparticles (NPs) [17][18], magnetic nanoparticles (NPs) [2], [19] and silica NPs [20]. Due to the high fabrication, application and regeneration costs of some of these adsorbents, scientific research is dedicated in developing low cost, easily applicable and regenerated adsorbents with high sorption capacity and efficiencies.

Graphene oxide (GO) offers interesting properties such as hydrophilicity due to the presence of carboxylic functional groups and epoxy groups essential for high sorption capacity [19]. This material has gained importance in portable and wastewater treatment due to its extraordinary properties such as its high adsorption capacity and catalysis efficiency [23]. GO can be composited with different inorganic materials and can also be incorporated into polymeric material through different interactions to improve its performance in water treatment applications [22]. The oxidation process during graphene oxide synthesis introduces hydrophilic groups for higher metal ion sorption capacity. In comparison to graphite, the GO carboxylic groups for functionalization in order to enhance the GO's surface properties [24] [17].

GO can also be functionalized to impact new properties such as the specificity, loading capacity solubility and biocompatibility [22]. Compositing GO with metal/ metal oxide does not only result in synergistic effects of the nanohybrids but also prevent the aggregation of the graphene oxide sheets [22]. Many researches have studied the properties of GO composited with metal oxides/ metals such as ZnO [25], SiO_2 [26], Fe_3O_4 [27], ZnSe [28], TiO_2 [29], [30], Ag [31], [32] and Pt [33]. Intercalating nanoparticles into graphene oxide sheets also enhances functionalities of the nanohybrids for processes such as photo-catalysis [30], adsorption [27], degradation [28],

and also improve the dispersibility and electro-conductivity of the nanocomposite.

Different types of adsorbents have been extensively exploited by research for the removal of heavy metals from water and wastewater. In most recent research, the application of nanocomposite polymeric membrane materials as adsorbents has been explored [34]-[35]. Polysulfone (PSf) is an engineering thermoplastic widely applied as an membrane material in separation techniques [36]. It is a popular polymeric material due to its excellent chemical and thermal stability, mechanical properties and aging resistant [37], [38]. However, PSf is not stable in aprotic solvents [39], therefore improving the solvent stability through internal crosslinking of the polymer is necessary.

PSf is relatively hydrophobic, and therefore prone to membrane fouling [40]. This is a major drawback especially in membrane filtration applications. Many methods have been applied to improve the properties of PSf for application in various fields. For instance, in a wide range of studies polysulfone has been modified by incorporating inorganic nanoparticles [41]–[44]. The incorporation of hydrophilic nanoparticles in PSf results in nanocomposite membranes with enhanced permeability, high porosity, high selectivity, improved hydrophilicity, and excellent fouling resistance [45]. However, the problem of membrane fouling is inevitable. Therefore, extensively exploiting the fouling process of nano-architectured membranes for adsorption purposes could be a necessary innovation. Another viable method is the preparation of composite membranes materials formed through polymer blending to achieve various property combinations of the resultant polymer blend [46].

This study is based on the synthesis and application of PSf/GO based nanohybrid membrane-based adsorbents for removal of metal ions in water. The main aim of the research is to investigate the interaction mechanism between the adsorbate and adsorbent. Objectives supporting this aim include comparing the adsorption capacity of the adsorbents, fitting adsorption data onto Langmuir and Freudlich isotherms, using kinetic studies to determine the rate of adsorption and characterizing the fabricated adsorbents.

2 METHODOLOGY

2.1 Materials

The graphite powder, potassium permanganate ($KMnO_4$), sulphuric acid (H_2SO_4), sodium nitrate ($NaNO_3$), hydrogen peroxide (H_2O_2), hydrochloric acid (HCl), zinc nitrate ($Zn(NO_3)_2$), formic acid (HCOOH), N-methyl-2-pyrrolidone (NMP), malic acid (MA) and polysulfone (PSf) were purchased from Sigma Aldrich. Deionized (DI) water was used throughout the experiments.

2.2 Preparation of graphene oxide

Graphene oxide was prepared from graphite powder by modified Hummers method reported by Li et al., (2012) [47] with minor modifications. The graphite powder was vigorously stirred with $NaNO_3$ in H_2SO_4 (95%), placed in an ice bath. $KMnO_4$ was gradually added in the solution over a period of 1 h under continuous stirring in an ice bath. The mixture was then stirred at room temperature for 5 days to complete the oxidation reaction. After the oxidation step, the temperature was gradually increased to 98 °C and the mixture was stirred for 2 h. The mixture was cooled at ambient conditions and H_2O_2 (30%) was added under constant stirring for 2 h. The mixture was centrifuged at 4200 rpm for 20 min and supernatant was decanted. The graphite oxide grains were washed with HCl (5%) and deionized water to remove impurities, exfoliated and oven dried.

2.3 Preparation of GO/ZnO nanohybrid

The GO/ZnO nanohybrid was synthesized using a method reported by Saravanakumar et al., (2012) [25]. Zinc oxide nanoparticles were prepared using a synthesis route reported by Gusati et al., (2009)[48]. The dried GO was dispersed in 200 mL of deionized water and sonicated for 30 min and KOH was then added to adjust the pH of the solution to pH 4. Zn $(NO_3)_2$ (0.2 M) was added drop-wise into the solution under vigorous stirring to ensure increased contact between the graphene oxide sheets and the zinc salt. The mixture was then stirred for 2 h and NH_4OH (25%) was added to adjust the pH of the mixture to pH 7 at 90 °C to improve the reaction between GO and ZnO. The mixture was centrifuged at 4200 rpm for 30 minutes and then the supernatant was decanted. The GO/ZnO nanohybrid was washed with DI water and oven dried. The product was calcined in the furnace for 2.5 h at 500 °C to crystalize the zinc oxide on the graphene oxide sheets to obtain the final product.

2.4 Preparation of GO/SiO_2 nanohybrid

The GO/SiO2 was synthesized using a modified preparation route reported by Maio et al., (2015) [26]. Silica nanoparticles were previously prepared using a modified sol-gel process reported by Tamba et al., (2015) [49] based on the classic Stober method. The GO and SiO2 were dispersed in DI water: HCOOH (2%) mixture in a ratio of 1:1and sonicated for 1 h. The dispersion was mechanically stirred at 120 °C for 1 h. The GO/SiO2 nanohybrid was dried overnight at 80 °C in the oven and calcined in the furnace for 2.5 h at 500 °C to crystalize the final product.

2.5 Fabrication of membrane-based adsorbents

The membrane- based adsorbent was prepared by the dissolution of PSf grains in NMP solution at 80 °C to obtain solution of a defined viscosity. A specified weight percentage (7.28 g) of malic acid (MA) was added drop-wise to obtain 25% crosslinking degree defined by Eq. "(1)".

$$X\% = \frac{W_{CL} \times MW_{PSf,Unit} \times 2}{W_{PSf} \times MW_{CL}} \times 100 \quad (1)$$

where WPSf and WCL represent the weight of PSf and the MA respectively, MWPSf, unit and MCL represent the molecular weight of the PSf monomer and that of the crosslinking agent. Hydrochloric acid (HCl) was added into the polymer matrix to hydrolyze the crosslinking agent.

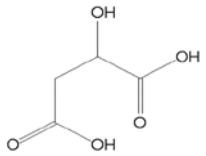

Fig. 1: Chemical structure of Malic Acid

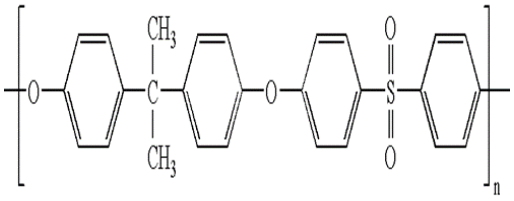

Fig. 2: Chemical Structure of PSf

The resulting solution was degassed overnight. Table 1 shows the loading ratios of the GO nanoparticles and metal oxide-graphene oxide nanohybrids into PSf matrices. The resulting matrix was casted onto petri dish and dried at 25 °C to evaporate the solvent. The thickness of the membranes was controlled to 2 mm using the Eq. "(2)" to calculate the volume of the casting solution

$$V = \pi r^2 h \tag{2}$$

2.6 Nanocomposite membrane film characterization

TABLE 1
FILLER LOADING RATES RATIOS

PSF (w.t %)	Filler loading rates (w.t %)
10	0
10	0.1
10	0.5

2.6.1 Water sorption tests

Water sorption tests were performed by the 'blot and weigh' immersion protocol. The membrane were cut into rectangular sheets, and dried in the oven for 24 h to ensure stable weight. The samples were then immersed in deionized water for 10 s, pressed between filter papers and weighed on an analytical balance at regular intervals until equilibrium was attained. This test is performed by measuring the amount of liquid absorbed by the fabricated membrane film as a function of time until saturation. The swelling rate was determined using Eq. "(3)":

$$Swellingrate = \frac{W_{wet} - W_{dry}}{W_{dry}} \tag{3}$$

where W_{wet} and W_{dry} are defined as the weight of swollen and dry samples respectively.

2.6.2 Batch adsorption experiments

The Adsorption of lead (Pb^{2+}) on the pristine membrane adsorbents impregnated with 0.001 and 0.005 % of GO, GOZnO and $GOSiO_2$ was performed at 298 k and shaking speed of 200 rpm using a batch mode experiment. Pb^{2+}, standards at concentrations of 10, 30 50, 100, 200 and 300 mg/L were each used with 1 (±0.02) cm^2 adsorbent in batch kinetic studies to investigate the effect of pH, contact time and initial concentration on the adsorption capacity/efficiency of the nanocomposite membranes.

The remaining concentration of the adsorbate was used to determine the adsorption capacity of the adsorbents, by using Eq. "(4):

$$q_t = \frac{(C_o - C_t)v}{W_s} \tag{4}$$

where q_t is the amount adsorbed at time t, C_t is the remaining concentration (ppm) at time t and C_o is the initial adsorbate concentration, v is the volume of the adsorbate solution (L) and w_s is the weight of the adsorbent (g).

The removal efficiency was calculated using Eq. "(5)":

$$\%Efficiency = \frac{C_o - C_e}{C_o} \times 100 \tag{5}$$

where C_o and C_e correspond to the initial concentration (mg/L) and equilibrium concentration (mg/L), respectively.

The equilibrium concentration q_e was determined by using isothermal experiments conducted using concentration of 50 mg/L, at pH 7. The experiments were performed for 6 h to allow equilibration at 20 ˚C. The equilibrium concentration q_e was calculated using Eq. "(4)":

$$q_e = \frac{(C_o - C_{e)v}}{C_o} \tag{6}$$

where: q_e is the adsorbed concentration at equilibrium, C_e is the equilibrium concentration (ppm) and W_s is the adsorbent mass. The other variables have the same meaning as in Eq. "(4)".

2.6.3 Surface properties of the GO based nanohybrids

Spectroscopic measurements were performed on a Perkin Elmer FTIR spectrometer (Frontier Optica) to confirm the successful attachment of the ZnO and SiO_2 onto the GO through functional group identification. The powdered nanoparticles were overlaid with a fine steel and pressed against the diamond. The FTIR spectra of the GO, $GOSiO_2$, and GOZnO are shown in figure 3.

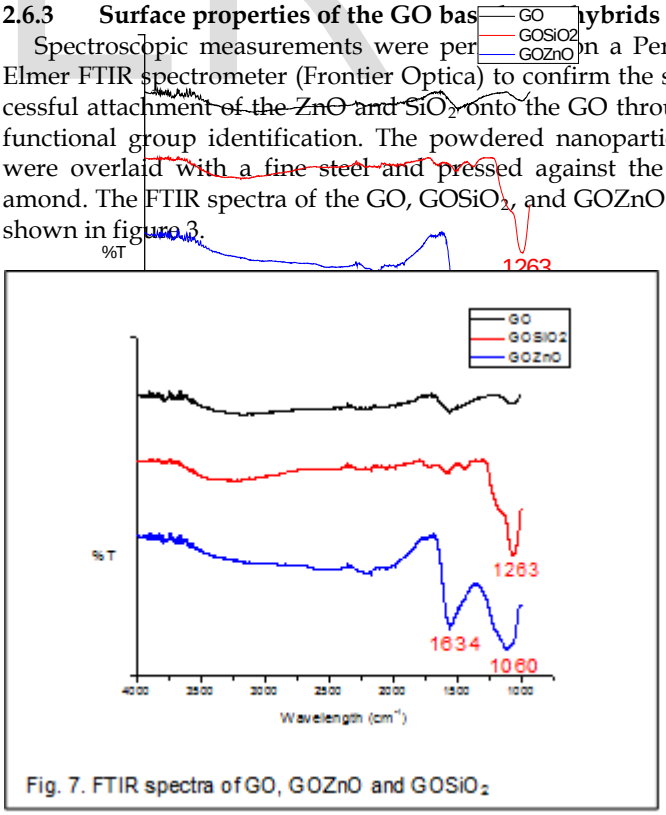

Fig. 7. FTIR spectra of GO, GOZnO and $GOSiO_2$

The surface and the charge of the nanoparticles were analyzed

using the Malvern zetasizer nanoseries. The nanoparticles were first dispersed in deionized ionized water and sonicated for 30 minutes and then analyzed in triplicates, 3 trials and the results from each trial were averaged.

2.6.4 Surface properties of the adsorbents

For surface morphology analysis of the membrane adsorbents, images of the membrane surfaces magnifications were obtained from scanning electron microscope (SEM) (JSM IT 300LV, JEOL) coupled with electron dispersive X-ray spectroscopy for elemental mapping. Sample preparation was done by coating the membrane samples with 10.2 mm of carbon using Quorum (Q150R ES).The zeta potential measurements of the adsorbents were done on the apical side of the membrane, using a current electrokinetic analyser (SurPass), equipped with a conductivity and a pH electrode, using 0.01 M KOH as an electrolyte. Water contact angle analysis were undertaken to determine the hydrophobic/hydrophilic properties of the membrane adsorbents.

3 RESULTS AND DISSCUSION

3.1 FTIR SPECTRA

Infrared spectrometric studies were performed in order to ascertain the purity and chemical composition of the nanoparticles. Metal oxides generally adsorb below the fingerprint region (below 1000 cm^{-1}). This corresponds to the adsorption bands given by GO-SiO_2 and GO-ZnO (in fig 4). The peaks at 1263 and 740 cm^{-1} in fig 4, correspond to Si-O_2 stretching and deformation vibrations. The peaks on the GO spectra (fig 4), can also be observed in the IR spectra for the GO-ZnO and GO-SiO_2 nanohybrid particles. Therefore this means that metal oxides were successfully calcined onto the graphene oxide to produce the nanohybrids. The most interesting bands are the peaks at 2250 - 3240 cm^{-1} corresponding to the O-H vibrations and stretching. Therefore the nanohybrids are hydrophobic due to the composition of OH groups, possibly a result of oxidation of graphite.

3.2 Zeta potential and size

The zeta potential and size of the nanoparticles were measured to determine the surface charge and the nanoparticle range of the nanohybrids. The results are tabulated in Table 2. The size of nanohybrids prepared varied in each trial and this may be due to aggregation of the nanoparticles and the different concentrations of the suspensions used in each trial. The size of the graphene oxide based nanoparticles exceeded the nanoparticle range; this is because due to the aggregation of graphene oxide sheets caused by the intercalated oxygen. However, the sizes of the GO-metal oxides were in the nanosize range which confirms that incorporating metal oxides in GO sheets prevents this aggregation [22]. The negative attribute of the nanoparticles suggest that the nanoparticles were hydrophilic. The hydrophilicity of the nanoparticles is due to polar groups including hydroxyl and carboxyl groups which will provides prerequisite heavy metals adsorption sites on the surface of GO sheets [3], [23], [51]. It is expected that during solvent evaporation phase inversion the nanoparticles will migrate to the membrane surface thus resulting in ionic interactions between the adsorbent surface and the heavy metals.

TABLE 2
SIZE AND ZETA POTENTIAL OF THE NANOHYBRIDS

Nanomaterial	Size (nm)	Zeta potential (mV)
GO	3138.0	-20.4
	6810.0	-19.7
GO-SiO2	3507.7	-13.9
	1092.75	-14.2
GO-ZnO	5390.3	-4.33
	5967.3	-2.3

3.3 Zeta potential of PSf membranes

The zeta potential of the PSF based adsorbents were found to be positive (Table 3). This is attributed to the polymer and the solvent as pure PSF is considered to be relatively non polar. Thus, resulting in the positive zeta potential of the adsorbents, as the polymer to nanofiller ratio is insignificant.

3.2 Contact angle

TABLE 3
ZETA POTENTIAL OF THE ADSORBENTS

Membrane	pH	Conductivity (mS/M)	Zeta potential (mV)
PSf	5.6	860.92	9.7
GO 0.01/PSf	5.6	486.92	20.09
GO 0.05/PSf	5.6	1314.24	35.61
GOZnO 0.01/PSf	5.6	1306.49	4.86
GOZnO 0.05/PSf	5.6	1407.79	29.27
GOSiO2 0.01/PSf	5.6	1327.34	7.21
$GOSiO_2$ /PSf	5.6	1314.24	20.09

The incorporation of GO based nanoparticles into the polysulfone membrane based adsorbents decreased the contact angle of the membranes thus improving the hydrophilicity of the adsorbents (Table 4). It was observed that the increase in nanofiller concentration (from 0.01 to 0.05 w.t %) also increased the hydrophilicity of the membranes. The improved hydrophilicity is indicated by the reduction in contact angles of the membranes. The effect of GO on hydrophobic PVDF membrane bioreactor (MBR) films membrane was reported by Zhao et al. (2014). The author's observed an improved surface hydrophilicity of the composite MBR membranes which was said to be due to the incorporation of hydrophilic GO sheets. [52]. The enhanced hydrophillicity was also observed by Rezaee and coworkers (2015) on arsenic rejecting PSf/GO

membranes [53]. The enhanced hydrophillicity was attributed to the dispersion of large amount of oxygen groups on the surface of the nanocomposite membranes caused by migration of nanoparticles to the membrane surface, resulting in a decreased interface energy with molecules [52]–[55].

Metal functionalized GO nanoparticles, in this case $GOSiO_2$

and GOZnO nanoparticles are also expected to exhibit the hydrophilic enhancing effect when embedded in hydrophobic membranes, as observed in the fabricated adsorbents. This is because silica and zinc oxide nanoparticles exhibits hydrophilic enhancement effect when incorporated in polymeric membranes [42],[56]. This may also be credited to the their ability to prevent the aggregation of the GO sheets [22], which may result in increased hydrophilic oxygen groups exposed on the adsorbent surfaces.

TABLE 4
CONTACT ANGLE OF MEMBRANE BASED ADSORBENTS

Membrane	Contact angle (°)
PSf	71.77
GO 0.01/PSf	64.66
GO 0.05/PSf	46.76
GOZnO 0.01/PSf	57.18
GOZnO 0.05/PSf	43.18
GOSiO2/PSf 0.01	55.62
$GOSiO_2$/PSf 0.05	40.93

3.5 Surface morphology

To investigate the surface morphologies of the membranes a typical scanning electron microscopy (SEM) was used to take the micrographs shown in Figure 4, after carbon coating.

The surface morphology of PSf membrane (fig 4 (c)) was observed to have uniformed pores with relatively the similar pore geometry. It can be observed from the SEM images (fig 4 (a), (b), (c)) that the incorporation of nanoparticles this disrupted uniform porosity. In these images (fig 4 (a), (b), (c)), membrane pores (or voids) with divergent pore geometry and incorporated nanoparticles can be observed on the surface of the membrane. This demonstrates that the nature of the nanohybrids exerts an effect in controlling the top surface morphology of the nanocomposite membrane. The porosity (void/surface ratio) of a membrane is one important aspect that facilitates the adsorption process as the adsorbate particles occupy the volume of the pores/voids[57], [58]

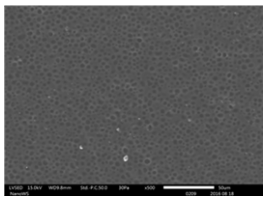

(a)

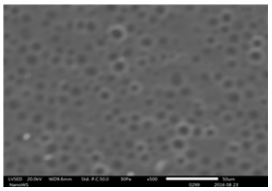

(b)

3.6 Swelling test

The swelling kinetics of the prepared PSf based adsorbent films are shown on Fig.8. The swelling equilibrium for the different adsorbents was attained. As expected, the water sorption of PSf increased as GO based nanohybrids were incorporated and more so at a higher concentration (0.05 w.t %) due to the increased interaction of hydrophilic membrane surface with the water molecules. Previous research by Ganesh et al., 2013, has established that increase in water up take of PSF/ Go membranes can be attributed to the different functional groups on GO surface, which ultimately imparts the overall membrane charge [55].The dissociation of carboxylic group attached to the graphitic back-bone and dissociation of the phenol groups are two main impacting on the membrane surface charge. Therefore, the increased water uptake can be attributed to the ion dipole water-membrane surface interaction caused the negatively charged ions on the membrane surface.

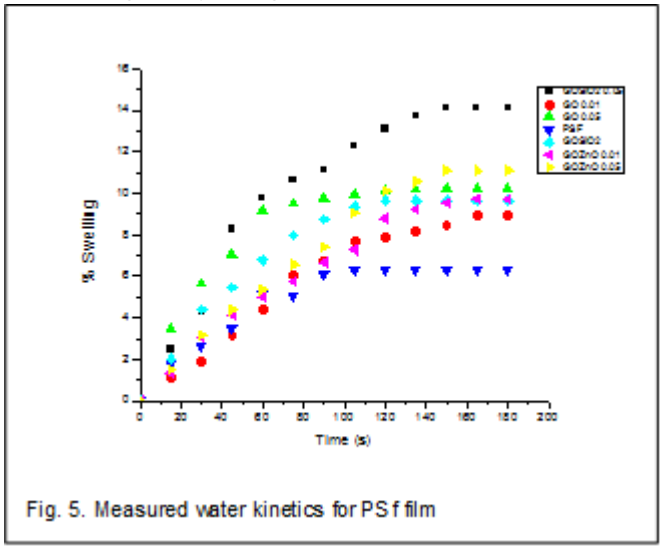

Fig. 5. Measured water kinetics for PS f film

3.6 Batch adsorption experiments

The sorption of lead (II) ions was observed to be significantly influenced by the pH due to the ionization of functional groups on the surface of the nanocomposite adsorbent. The adsorption capacity of pure PSf was high at pH=5 (Fig. 6). The high adsorption capacity was due to hydrophobic interactions

(Van der Waals and London forces), since the PSf membranes were moderately hydrophobic, this concurs with the contact angle results reported in Table 4.

The pH in these experiments was varied from ±3 to ±9 (fig 7). The adsorption capacity of the Pb^{2+} ions by nanocomposite membranes was observed to be low at acidic pH±5 due to the significantly high concentration of hydrogen ions. The assumption is that the positively charged hydrogen ions compete with the heavy metals for binding on the nanocomposite adsorbent surface. Therefore fewer active binding sites were available for the sorption of Pb^{2+} ions. The maximum adsorption capacity was observed at alkaline pH = ±9 due to the negative charge introduced by OH^- groups on the functional groups of the membrane adsorbents and also due to the decrease in hydrogen species which competed with lead ions at acidic pH.

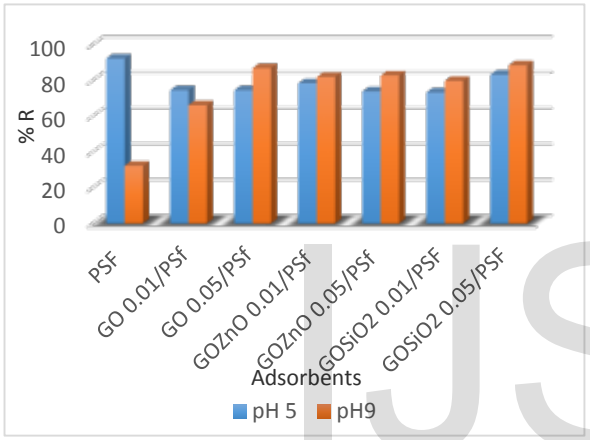

Fig. 6. Removal efficiency as a function of pH

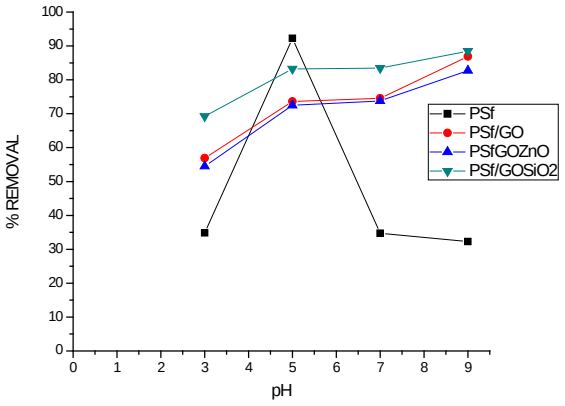

Fig. 7. Effect of pH on adsorption capacity

The effect of initial concentration was studied for all the adsorbents, Fig. 8. (a) and (b). It was observed that the adsorption capacity increased as the analyte concentration increased; as can be seen in Fig. 8. (a) and (b). This is attributed to the increased availability of Pb^{2+} ions in the solution which increases the frequency of contact and interactions between adsorbate and adsorbent. The effect surface modification of the membrane adsorbents.

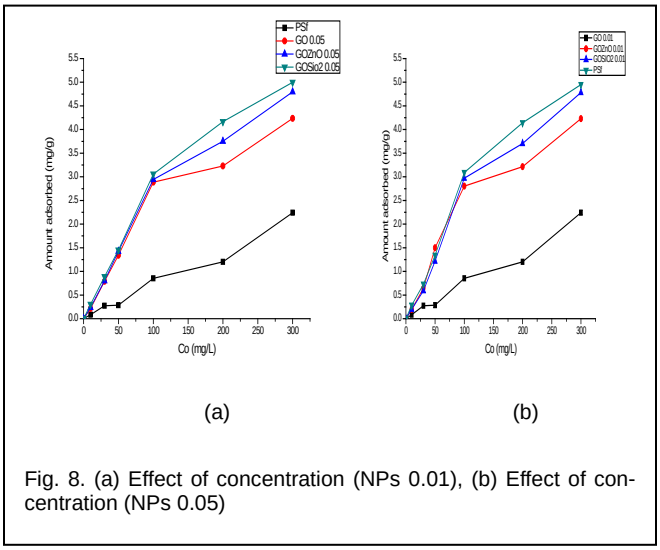

Fig. 8. (a) Effect of concentration (NPs 0.01), (b) Effect of concentration (NPs 0.05)

The effect of initial concentration was studied for all the adsorbents, Fig. 8. (a) and (b). It was observed that the adsorption capacity increased as the analyte concentration increased; as can be seen in Fig. 8. (a) and (b). This is attributed to the increased availability of Pb^{2+} ions in the solution which increases the frequency of contact and interactions between adsorbate and adsorbent. The effect surface modification of the membrane adsorbents

The absorption capacity of the nanocomposites was evaluated as a function of time and filler concentration (Figure 8 (a) and (b)). It can be observed that the adsorption capacity of the nanocomposite adsorbents was enhanced. This is attributed to polar groups including hydroxyl and carboxyl groups of GO sheets which will provides prerequisite heavy metals adsorption sites on the membrane surface [53]. The enhance removal of lead (Pb^{2+}) ions may be ascribed to the ionic interaction between Pb^{2+} ions and the hydroxyl and carboxyl radicals of GO dispersed on the membrane surfaces. The $GOSiO_2$ nanocomposite adsorbent had the highest adsorption capacity compared to GOZnO nanocomposite even though they are both metal oxide composites. This is attributed to the silanol groups on the surface of silica particles [59] responsible for the increased adherence of lead ions onto the adsorbent. The influence of nanofiller concentration on the adsorption capacity was also observed in figure 10 and 11. It was observed that as the nanofiller concentration was increased from 0.01 wt. % to 0.05 wt. %, the adsorption capacity increased. This is due to the increased availability of active sorption sites on the surface of the membrane.

The effect of contact time illustrated by Fig. 9 (a) and (b), was studied for a period of 24 hours. It can be clearly seen that the adsorption capacity of lead ions from the aqueous solutions was rapid at the beginning and this is attributed to the high number of vacant available active sites. However, as the adsorption processes continued the amount adsorbed gradually decreased until all the vacant sites were occupied, reaching a

saturation point. Furthermore, one can take note that increase of nanofiller content in the composite membranes lead to a higher adsorption capacity. This demonstrates that the adsorption ability of nanocomposite membranes was enhanced due to the incorporation of Go nanohybrids.

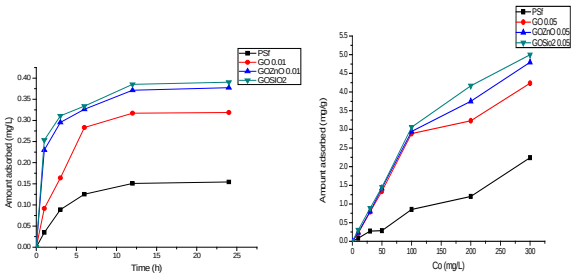

(a) (b)

Fig. 9. (a) Effect of concentration (NPs 0.01), (b) Effect of concentration (NPs 0.05)

3.7 Adsorption Isotherms

The adsorption data of Pb^{2+} ions were fitted into Langmuir and Freundlich models for the description of Pb^{2+} ions uptake under conditions studied. The fitted Langmuir and Freundlich graphs are shown in Fig.10 and 11, respectively.

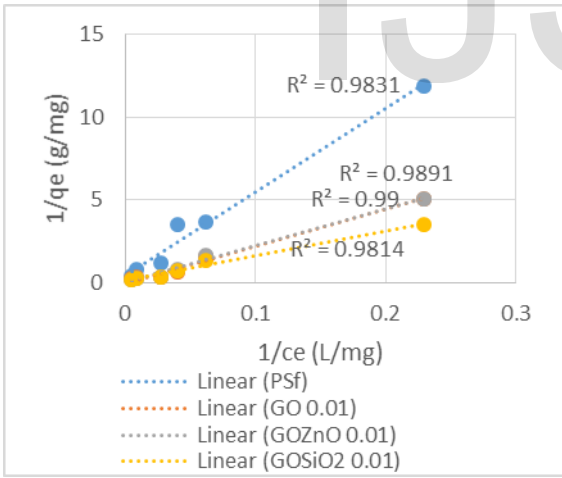

Fig. 10(a). Langmuir adsdorption isotherm (0.01w.t %)

The adsorption isotherms of lead (II) ions by the membrane adsorbents were studied using initial concentrations from 10 to 200 mg/L. The adsorption isotherms used in this study interprets the adsorption capacity as a function of the final concentration. The batch equilibrium data were linearized by fitting into the Langmuir and Freundlich isotherm theorems (Fig. 10 and 11).The Langmuir isotherm is based on the assumption that the adsorbent surface has finite adsorption sites [60]. When these site are occupied, then the adsorption equilibrium has been reached (exchange of solute between the adsorbent and the solution) [61]. The linearized form of the Langmuir isotherm is expresses in Eq. "(7)", as follows:

$$\frac{1}{q_e} = \left[\frac{1}{K_L q_{\max}}\right]\frac{1}{C_e} + \frac{1}{q_{\max}} \qquad (7)$$

where q_e and q_{max} are the defined as the amount adsorbed at equilibrium (mg/g) and theoretical adsorption capacity of the adsorbents (mg/g), respectively. K_L is the Langmuir affinity constant and C_e is the equilibrium concentration of the Pb^{2+} in solution. A plot of $1/q_e$ versus $1/C_e$ from the adsorption data is expected to give a straight line to confirm the Langmiur assumptions to be true.

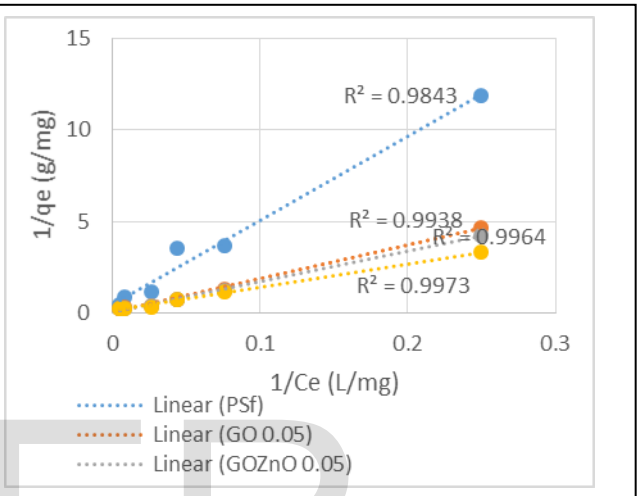

Fig. 10(b). Langmuir adsorption isotherm (0.05w.t %)

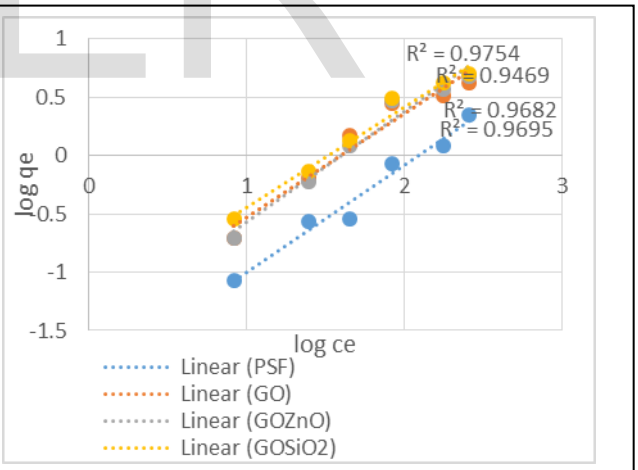

Fig. 11(a). Freundlich isotherm (0.01w.t %)

The Freundlich isotherm on the other hand is based on the assumption that adsorption occurs on a heterogeneous surface implying multi-layer adsorption [62].This isotherm predicts that the adsorbate concentration will increase as the initial concentration of the solution is increased [63]. The linearized form of the Freundlich isotherm is expressed in Equation 8, as follows:

$$\log q_e = \log K_f + \frac{1}{n}\log C_e \qquad (8)$$

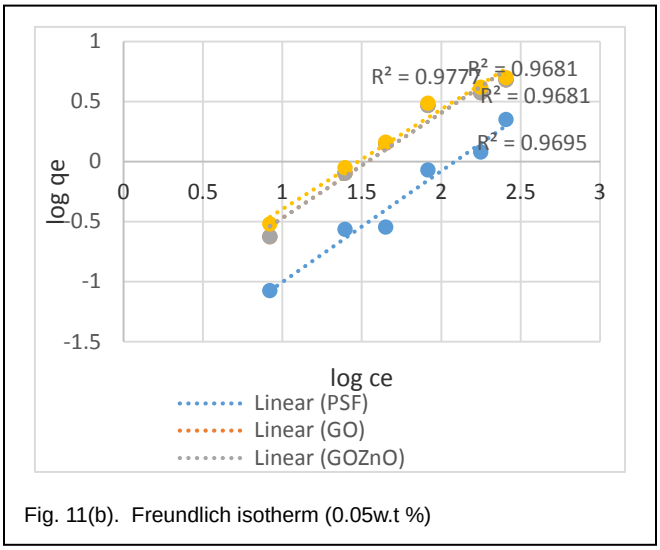

Fig. 11(b). Freundlich isotherm (0.05w.t %)

A straight line fit obtained from the plot of *log* q_e against *log* C_e for the Freundlich model assumes the hypothesis as true. K_f is defined as the Freundlich constant related to the adsorption capacity (mg/g), n is associated with the adsorption intensity which varies with the heterogeneity of adsorbent and therefore establishes the favourability of the adsorbate/adsorbent system.

The correlation coefficients (R2) of the graphs represented by Fig. 10-11, were compared to confirm which isotherm model fits the adsorption data. The R^2 values obtained from the Langmuir models were higher than those obtained from the Freundlich model. This implies that the Langmuir isotherm model is the most suitable for the fitting of the adsorption data. The favourability of the adsorbate/adsorbent system was calculated using the Freundlich adsorption model.

TABLE 5
LANGMUIR AND FREUNDLICH ADSORPTION ISOTHERM PARAMETERS.

PSf Adsorbents	Langmuir constants			Freundlich constants		
	q_{max} (mg/g)	K_L (L/mg)	R^2	K_f (mg/g)	n (L/mg)	R^2
PSf	0.306	96.285	0.9831	0.9288	1.9283	0.9695
GO 0.01	0.2048	31.374	0.9814	0.8068	1.16318	0.9469
GO 0.05	0.1426	26.592	0.99	0.8915	1.1619	0.9681
GOZnO 0.01	0.1378	31.624	0.9891	0.9068	1.2919	0.9482
GOZNO 0.05	0.1872	22.254	0.9964	0.9062	1.1537	0.9681
$GOSiO_2$ 0.01	0.1413	14.870	0.9831	0.7705	0.9729	0.9754
$GOSiO_2$ 0.05	0.1921	13.288	0.9930	0.8017	0.9473	0.9777

The n values obtained from fitting the data onto Freundlich isotherm were greater than one, except for PSf/$GOSiO_2$ membrane adsorbent. This means that the adsorption process for the PSf/GOSiO2 membranes is due to chemisorption and is regarded as favourable. However, for the other membrane adsorbents, the adsorption process is considered as unfavourable and is due to physisorption. The Langmuir and Freundlich adsorption parameters are reported in Table 5.

3.8 Adsorption kinetics

The The Langergren pseudo first order and pseudo second order kinetic models for the description of PNP adsorption data determined under conditions studied. This is shown in Figure 12 and 13, respectively.

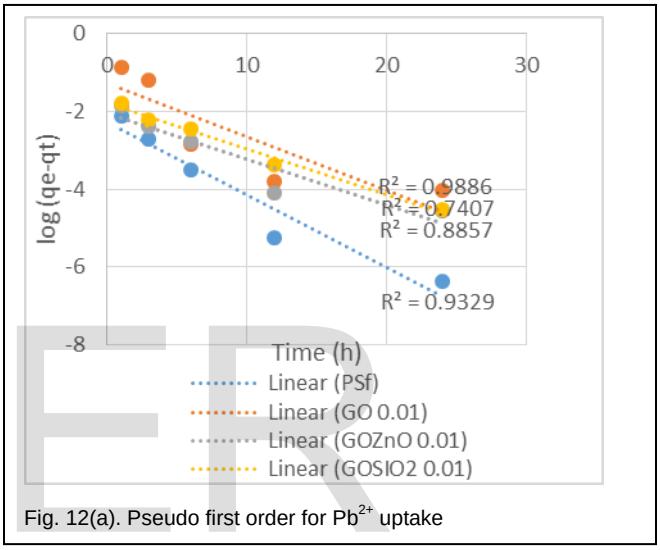

Fig. 12(a). Pseudo first order for Pb^{2+} uptake

Kinetic models were used to determine the adsorption rate of 50 mg/L Pb^{2+} ions under time variation of 24 h .This is one important aspect which determines the efficiency of adsorbents. The Langergren pseudo first order and pseudo second order kinetic models were used in this study (Fig. 12 and 13). The fitting of the experimental data into kinetic models is essential for the deduction of the adsorption rate, model the adsorption process and predict information about adsorbent and adsorbate interaction [62], [64]. The pseudo first order equation can be expressed in Eq. "(9)" as follows:

$$\frac{d_q}{d_t} = K_1(q_e - q_t) \quad (9)$$

q_e and q_t are defined as the amount adsorbed (mg/g) at equilibrium and time t, respectively and k_1 is the rate constant of the pseudo first order kinetic model. The integrated form of this equation becomes:

$$\ln(q_e - q_t) = \ln q_e - \frac{k_1}{2.303}t \quad (10)$$

A plot of $ln\ (q_e - q_t)$ against t should give a linear graph for the pseudo first order model to be applicable.

The second order kinetic equation is expressed as:

$$\frac{d_q}{d_t} = k_2(q_e - q_t)^2 \quad (11)$$

k_2 is defined as the rate constant of the pseudo second order adsorption kinetic model. The kinetic adsorption parameters are tabulated in Table 8 and 9 for the first order and second order, respectively.

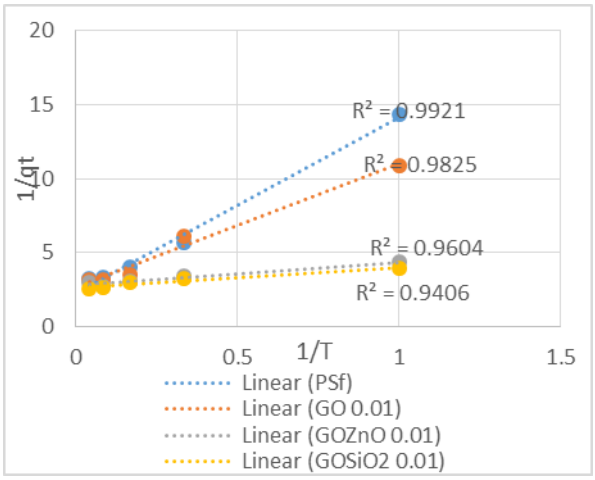

Fig. 12(b). Pseudo second order for Pb^{2+} uptake

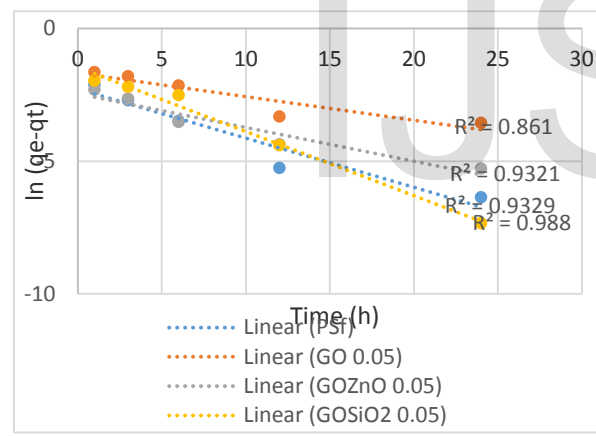

Fig. 13(a). Pseudo first order for Pb^{2+} uptake (0.05)

The R^2 of the GO (0.01), (GO 0.05) and GOZnO (0.01) were below the minimum value (0.9) when fitted to the Langregan pseudo first order kinetic model. This implies that the adsorption kinetic data from these adsorbents does not obey pseudo first order kinetics law. R^2 from adsorptive data obtained using GO (0.05) and $GOSiO_2$ were below 0.9 which means the data does not obey the pseudo second order adsorption model. In both cases, the experimental adsorption capacity (q_e) was incomparable with the calculated adsorption capacity (q_c). Therefore, the data cannot be fitted onto the first and second order kinetic models implying that adsorption rate of the lead ions onto the adsorbents does not obey the pseudo first order and the pseudo second order. This means that the uptake of lead ions resulting in adsorbate-adsorbent complexes is not influenced by the total number of active sites nor no the initial concentration of the pollutant. With these results, it can be concluded that the ionic interactions could not singly impact on the adsorption rate [61]. Therefore intra particle diffusion of the adsorbate ions into the membrane pores could possibly affect the adsorption process.

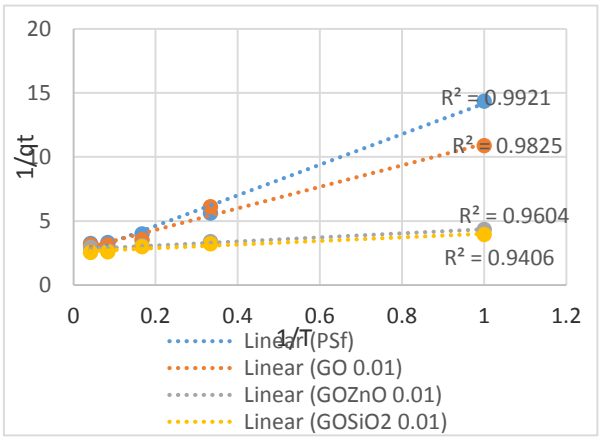

Fig. 13(b). Pseudo second order for Pb^{2+} uptake (0.05)

4 Conclusion

From the results obtained, it was observed that lead (II) ions uptake in aqueous solutions was greatly affected by the pH of the solution, Pb^{2+} initial concentration and contact time with the adsorbents. The maximum uptake by PSf adsorbents occurred at pH 5. However, for the other nanocomposite adsorbents, maximum adsorption occurred at pH 9. The Lang-

TABLE 8
PSEUDO FIRST ORDER ADSORPTION KINETICS PARAMETERS FOR Pb^{2+} UPTAKE

Adsorbent	q_e exp (mg/L)	q_e calc (mg/L)	k_1 (min^{-1})	R^2
PSf	0.0156	2.2759	0.1858	0.9329
GO (0.01)	0.323	1.663	0.2348	0.7407
GO (0.05)	0.751	1.6804	0.0887	0.8610
GOZnO (0.01)	0.338	2.055	0.01169	0.8857
GOZnO (0.05)	0.385	2.5001	0.01669	0.9329
$GOSiO_2$ (0.01)	0.421	0.8265	0.1169	0.9880
$GOSiO_2$ (0.05)	0.048	1.4587	0.242	0.9886

TABLE 9
PSEUDO SECOND ORDER ADSORPTION PARAMETERS FOR Pb^{2+}

Adsorbent	q_e exp (mg/L)	q_e calc (mg/L)	k_2 (min^{-1})	R^2
PSf	0.0156	2.2298	11.929	0.9921
GO (0.01)	0.323	2.6393	8.3876	0.9825
GO (0.05)	0.751	2.923	0.79449	0.824
GOZnO (0.01)	0.338	2.664	1.735	0.9703
GOZnO (0.05)	0.385	2.6746	0.8855	0.8918
$GOSiO_2$ (0.01)	0.421	2.615	1.3935	0.9406
$GOSiO_2$ (0.05)	0.048	2.5658	1.1253	0.7658

muir adsorption isotherm was suitable to describe the adsorption process of lead (II) ions onto the adsorbent, which suggested monolayer adsorption mechanism. Langragen pseudo first order and second order were used to analyse the kinetic data. From the pseudo first order kinetics model a better correlation was obtained as compared to the second order model. However, experimental q_e and calculated q_e were not comparable. From this study it was demonstrated that membrane adsorbent can be used for adsorption purposes, and the adsorption capacity is more or less comparable to that obtained from studies whereby nanoparticles were used. Even though ionic interactions between the adsorbate and adsorbent were an integral part of the adsorption process, the diffusion of lead ions into voids/pores (seen in SEM images) resulted in an increased adsorption capacity.

7.2 Acknowledgments

The authors acknowledge the financial support from the University of South Africa (UNISA) and the Nanotechnology and Water Sustainability (NanoWS) research unit, and SASOL.

REFERENCES

[1] M. A. Barakat, "New trends in removing heavy metals from industrial wastewater," *Arab. J. Chem.*, vol. 4, no. 4, pp. 361–377, 2011.

[2] F. Ge, M.-M. Li, H. Ye, and B.-X. Zhao, "Effective removal of heavy metal ions Cd2+, Zn2+, Pb2+, Cu2+ from aqueous solution by polymer-modified magnetic nanoparticles," *J. Hazard. Mater.*, vol. 211–212, pp. 366–372, 2012.

[3] P. Tan, J. Sun, Y. Hu, Z. Fang, Q. Bi, Y. Chen, and J. Cheng, "Adsorption of Cu2+, Cd2+ and Ni2+ from aqueous single metal solutions on graphene oxide membranes," *J. Hazard. Mater.*, vol. 297, pp. 251–260, 2015.

[4] B. Al-Rashdi, C. Somerfield, and N. Hilal, "Heavy Metals Removal Using Adsorption and Nanofiltration Techniques," *Sep. Purif. Rev.*, vol. 40, no. 3, pp. 209–259, 2011.

[5] M. Kamib, A. Kabbani, H. Holail, and Z. Olama, "Heavy metals removal using activated carbon, silica and silica activated carbon composite," *Energy Procedia*, vol. 50, pp. 113–120, 2014.

[6] V. K. Gupta and I. Ali, *Chapter 2 - Water Treatment for Inorganic Pollutants by Adsorption Technology*. 2013.

[7] Ihsanullah, A. Abbas, A. M. Al-Amer, T. Laoui, M. J. Al-Marri, M. S. Nasser, M. Khraisheh, and M. A. Atieh, "Heavy metal removal from aqueous solution by advanced carbon nanotubes: Critical review of adsorption applications," *Sep. Purif. Technol.*, vol. 157, pp. 141–161, 2016.

[8] W. Griswold and S. Martin, "Human Health Effects of Heavy Metals," *Environ. Sci. Technol.*, no. 15, pp. 1–6, 2009.

[9] R. Singh, N. Gautam, A. Mishra, and R. Gupta, "Heavy metals and living systems: An overview.," *Indian J. Pharmacol.*, vol. 43, no. 3, pp. 246–53, May 2011.

[10] G. (Gordon) McKay, *Use of adsorbents for the removal of pollutants from wastewaters*. CRC Press, 1996.

[11] S. K. Gunatilake, "Methods of Removing Heavy Metals from Industrial Wastewater," *J. Multidiscip. Eng. Sci. Stud.*, vol. 1, no. 1, pp. 12–18, 2015.

[12] J. Wang and B. Chen, "Adsorption and coadsorption of organic pollutants and a heavy metal by graphene oxide and reduced graphene materials," *Chem. Eng. J.*, vol. 281, pp. 379–388, 2015.

[13] Gunatilake SK, "Methods of Removing Heavy Metals from Industrial Wastewater," *J. Multidiscip. Eng. Sci. Stud.*, vol. 1, no. 1, pp. 2912–1309, 2015.

[14] M. Mudasir, K. Karelius, N. H. Aprilita, and E. T. Wahyuni, "Adsorption of mercury(II) on dithizone-immobilized natural zeolite," *J. Environ. Chem. Eng.*, vol. 4, no. 2, pp. 1839–1849, 2016.

[15] X. Luo, Z. Zhang, P. Zhou, Y. Liu, G. Ma, and Z. Lei, "Synergic adsorption of acid blue 80 and heavy metal ions (Cu2+/Ni2+) onto activated carbon and its mechanisms," *J. Ind. Eng. Chem.*, vol. 27, pp. 164–174, 2015.

[16] Z. Guo, J. Fan, J. Zhang, Y. Kang, H. Liu, L. Jiang, and C. Zhang, "Sorption heavy metal ions by activated carbons with well-developed microporosity and amino groups derived from Phragmites australis by ammonium phosphates activation," *J. Taiwan Inst. Chem. Eng.*, vol. 58, pp. 290–296, 2016.

[17] A. Gopalakrishnan, R. Krishnan, S. Thangavel, G. Venugopal, and S. J. Kim, "Removal of heavy metal ions from pharma-effluents using graphene-oxide nanosorbents and study of their adsorption kinetics," *J. Ind. Eng. Chem.*, vol. 30, pp. 14–19, 2015.

[18] L. P. Lingamdinne, J. R. Koduru, H. Roh, Y. L. Choi, Y. Y. Chang, and J. K. Yang, "Adsorption removal of Co(II) from waste-water using graphene oxide," *Hydrometallurgy*, 2015.

[19] S. Kango and R. Kumar, "Low-cost magnetic adsorbent for As(III) removal from water: adsorption kinetics and isotherms," *Environ. Monit. Assess.*, vol. 188, no. 1, pp. 1–14, 2016.

[20] M. Xu, J. Liu, K. Hu, C. Xu, and Y. Fang, "Nickel(II) removal from water using silica-based hybrid adsorbents: Fabrication and adsorption kinetics," *Chinese J. Chem. Eng.*, no. Ii, 2016.

[21] S. M. Notley and D. R. Evans, "Aqueous processing of graphene-polymer hybrid thin film nano-composites and gels," *Adv. Colloid Interface Sci.*, vol. 209, pp. 196–203, 2014.

[22] Wang, X. Yuan, Y. Wu, H. Huang, X. Peng, G. Zeng, H. Zhong, J. Liang, and M. M. Ren, "Graphene-based materials: Fabrication, characterization and application for the decontamination of wastewater and wastegas and hydrogen storage/generation," *Adv. Colloid Interface Sci.*, vol. 195–196, pp. 19–40, 2013.

[23] X. hao Liu, J. Duan, J. hui Yang, T. Huang, N. Zhang, Y. Wang, and Z. wan Zhou, "Hydrophilicity, morphology and excellent adsorption ability of poly(vinylidene fluoride) membranes induced by graphene oxide and polyvinylpyrrolidone," *Colloids Surfaces A Physicochem. Eng. Asp.*, vol. 486, pp. 172–184, 2015.

[24] Mabayoje, M. Seredych, and T. J. Bandosz, "Enhanced Reactive Adsorption of Hydrogen Sulfide on the Composites of Graphene/Graphite Oxide with Copper (Hydr)oxychlorides," 2012.

[25] B. Saravanakumar, R. Mohan, and S. J. Kim, "Facile synthesis of graphene/ZnO nanocomposites by low temperature hydrothermal method," *Mater. Res. Bull.*, vol. 48, no. 2, pp. 878–883, 2013.

[26] A. Maio, S. Agnello, R. Khatibi, L. Botta, A. Alessi, A. Piazza, G. Buscarino, A. Mezzi, G. Pantaleo, and R. Scaffaro, "A rapid and eco-friendly route to synthesize graphene-doped silica nanohybrids," *J. Alloys Compd.*, vol. 664, pp. 428–438, 2015.

[27] Y. Zhang, B. Chen, L. Zhang, J. Huang, F. Chen, Z. Yang, J. Yao, and Z. Zhang, "Controlled assembly of Fe3O4 magnetic nanoparticles on graphene oxide.," *Nanoscale*, vol. 3, no. 4, pp. 1446–50, 2011.

[28] S. H. Hsieh, W. J. Chen, and T. H. Yeh, "Effect of various amounts of graphene oxide on the degradation characteristics of the ZnSe/graphene nanocomposites," *Appl. Surf. Sci.*, vol. 358, pp. 63–69, 2015.

- *N.P. Khumalo is a masters student currently affiliated Nanotechnology and Water Sustainability (NanoWS) unit at the University of South Africa, South Africa, E-mail: author_khumalocceh@gmail.com*
- *Corresponding Author: DS Dlamini Is currently affiliated Nanotechnology and Water Sustainability (NanoWS) unit at the University of South Africa, South Africa, E-mail: author_dlamisd@unisa.ac.za*

[29] C. Xu, A. Cui, Y. Xu, and X. Fu, "Graphene oxide-TiO2 composite filtration membranes and their potential application for water purification," *Carbon N. Y.*, vol. 62, pp. 465–471, 2013.

[30] V. Stengl, S. Bakardjieva, T. M. Grygar, J. Bludská, and M. Kormunda, "TiO2-graphene oxide nanocomposite as advanced photocatalytic materials.," *Chem. Cent. J.*, vol. 7, no. 1, p. 41, 2013.

[31] J. Chen, X. Zheng, H. Wang, and W. Zheng, "Graphene oxide-Ag nanocomposite: In situ photochemical synthesis and application as a surface-enhanced Raman scattering substrate," *Thin Solid Films*, vol. 520, no. 1, pp. 179–185, 2011.

[32] J. Yang, C. Zang, L. Sun, N. Zhao, and X. Cheng, "Synthesis of graphene/Ag nanocomposite with good dispersibility and electroconductibility via solvothermal method," *Mater. Chem. Phys.*, vol. 129, no. 1–2, pp. 270–274, 2011.

[33] R. Kempegowda, D. Antony, and P. Malingappa, "Graphene–platinum nanocomposite as a sensitive and selective voltammetric sensor for trace level arsenic quantification," *Int. J. Smart Nano Mater.*, vol. 5, no. 1, pp. 17–32, 2014.

[34] A. R. Keshtkar, M. Irani, and M. A. Moosavian, "Comparative study on PVA/silica membrane functionalized with mercapto and amine groups for adsorption of Cu(II) from aqueous solutions," *J. Taiwan Inst. Chem. Eng.*, vol. 44, no. 2, pp. 279–286, 2013.

[35] J. Liu, X. Wang, T. Xu, and G. Shao, "Novel negatively charged hybrids. 1. copolymers: Preparation and adsorption properties," *Sep. Purif. Technol.*, vol. 66, no. 1, pp. 135–142, 2009.

[36] L. Y. Ng, C. P. Leo, and A. W. Mohammad, "Optimizing the incorporation of silica nanoparticles in polysulfone/poly(vinyl alcohol) membranes with response surface methodology," *J. Appl. Polym. Sci.*, vol. 121, no. 3, pp. 1804–1814, Aug. 2011.

[37] P. Wankat, "Separation process engineering," 2006.

[38] J. H. Jhaveri and Z. V. P. Murthy, "A comprehensive review on anti-fouling nanocomposite membranes for pressure driven membrane separation processes," *Desalination*, vol. 379, pp. 137–154, 2016.

[39] D. Chen, X. Liu, D. Li, and X. Li, "Highly stable polysulfone solvent resistant nanofiltration membranes with internal cross-linking networks," *RSC Adv.*, vol. 6, no. 35, pp. 29570–29575, 2016.

[40] D. S. Dlamini, J. Wang, A. K. Mishra, B. B. Mamba, and E. M. V. Hoek, "Effect of Cross-Linking Agent Chemistry and Coating Conditions on Physical, Chemical, and Separation Properties of PVA-Psf Composite Membranes," *Sep. Sci. Technol.*, vol. 49, no. 1, pp. 22–29, 2014.

[41] S. Habibi, A. Nematollahzadeh, and S. A. Mousavi, "Nano-scale modification of polysulfone membrane matrix and the surface for the separation of chromium ions from water," *Chem. Eng. J.*, vol. 267, pp. 306–316, 2015.

[42] H. L. Richards, P. G. L. Baker, and E. Iwuoha, "Metal Nanoparticle Modified Polysulfone Membranes for Use in Wastewater Treatment: A Critical Review," *J. Surf. Eng. Mater. Adv. Technol.*, vol. 2, no. 3, pp. 183–193, 2012.

[43] R. S. Zambare, K. B. Dhopte, A. V. Patwardhan, and P. R. Nemade, "Polyamine functionalized graphene oxide polysulfone mixed matrix membranes with improved hydrophilicity and anti-fouling properties," *Desalination*, pp. 11–15, 2016.

[44] P. C. Bernardes, N. J. de Andrade, L. H. M. da Silva, A. F. de Carvalho, P. É. Fernandes, E. A. Araújo, C. A. Lelis, P. C. G. Mol, and J. P. N. de Sá, "Modification of polysulfone membrane used in the water filtration process to reduce biofouling.," *J. Nanosci. Nanotechnol.*, vol. 14, no. 8, pp. 6355–67, Aug. 2014.

[45] J. Garcia-Ivars, M.-I. Iborra-Clar, M.-I. Alcaina-Miranda, and B. Van der Bruggen, "Comparison between Hydrophilic and Hydrophobic metal nanoparticles on the phase separation phenomena during formation of asymmetric polyethersulphone membranes," *J. Memb. Sci.*, vol. 493, pp. 709–722, 2015.

[46] V. Kochkodan and N. Hilal, "A comprehensive review on surface modified polymer membranes for biofouling mitigation," *Desalination*, vol. 356, pp. 187–207, 2015.

[47] B. Li, T. Liu, Y. Wang, and Z. Wang, "ZnO/graphene-oxide nanocomposite with remarkably enhanced visible-light-driven photocatalytic performance," *J. Colloid Interface Sci.*, vol. 377, no. 1, pp. 114–121, 2012.

[48] M. Gusatti, J. Rosário, and G. Barroso, "Synthesis of ZnO nanostructures in low reaction temperature," *Chem. Eng. …*, 2009.

[49] B. I. Tamba, A. Dondas, M. Leon, A. N. Neagu, G. Dodi, C. Stefanescu, and A. Tijani, "Silica nanoparticles: Preparation, characterization and in vitro/in vivo biodistribution studies," *Eur. J. Pharm. Sci.*, vol. 71, pp. 46–55, 2015.

[50] D. S. Dlamini, S. Levchenko, M. Bass, B. B. Mamba, E. M. V Hoek, J. M. Thwala, and V. Freger, "Solute hindrance in non-porous membranes: An ATR-FTIR study," *Desalination*, vol. 368, pp. 60–68, 2015.

[51] S. Pourbeyram, "Effective Removal of Heavy Metals from Aqueous Solutions by Graphene Oxide−Zirconium Phosphate (GO−Zr-P) Nanocomposite."

[52] C. Zhao, X. Xu, J. Chen, G. Wang, and F. Yang, "Highly effective antifouling performance of PVDF/graphene oxide composite membrane in membrane bioreactor (MBR) system," *Desalination*, vol. 340, no. 1, pp. 59–66, 2014.

[53] R. Rezaee, S. Nasseri, A. H. Mahvi, R. Nabizadeh, S. A. Mousavi, A. Rashidi, A. Jafari, and S. Nazmara, "Fabrication and characterization of a polysulfone-graphene oxide nanocomposite membrane for arsenate rejection from water," *J. Environ. Heal. Sci. Eng.*, vol. 13, no. 1, p. 61, 2015.

[54] M. E. A. Ali, L. Wang, X. Wang, and X. Feng, "Thin film composite membranes embedded with graphene oxide for water desalination," *Desalination*, vol. 386, pp. 67–76, 2016.

[55] B. M. Ganesh, A. M. Isloor, and A. F. Ismail, "Enhanced hydrophilicity and salt rejection study of graphene oxide-polysulfone mixed matrix membrane," *Desalination*, vol. 313, pp. 199–207, 2013.

[56] A. Peyki, A. Rahimpour, and M. Jahanshahi, "Preparation and characterization of thin film composite reverse osmosis membranes incorporated with hydrophilic SiO2 nanoparticles," *Desalination*, vol. 368, pp. 152–158, 2014.

[57] A. S. Chuck and B. Ø. Palsson, "Membrane adsorption characteristics determine the kinetics of flow- through transductions," *Biotechnol. Bioeng.*, vol. 51, no. 3, pp. 260–270, 1996.

[58] C. Boi, S. Dimartino, and G. C. Sarti, "Modelling and simulation of affinity membrane adsorption," *J. Chromatogr. A*, vol. 1162, no. 1 SPEC. ISS., pp. 24–33, 2007.

[59] J. Kujawa, A. Rozicka, S. Cerneaux, and W. Kujawski, "The influence of surface modification on the physicochemical properties of ceramic membranes," *Colloids Surfaces A Physicochem. Eng. Asp.*, vol. 443, pp. 567–575, 2014.

[60] D. S. Dlamini, A. K. Mishra, and B. B. Mamba, "Kinetic and equilibrium studies of the removal of Pb2+ from aqueous solutions using Na2SO4-EVA/Cloisite® 20A composite," *Mater. Chem. Phys.*, vol. 133, no. 1, pp. 369–375, 2012.

[61] T. M. Elmorsi, Z. H. Mohamed, W. Shopak, and A. M. Ismaiel, "Kinetic and Equilibrium Isotherms Studies of Adsorption of Pb (II) from Water onto Natural Adsorbent," *J. Environ. Prot. (Irvine,. Calif).*, no. 5, pp. 1667–1681, 2014.

[62] A. K. Bhattacharya, T. K. Naiya, S. N. Mandal, and S. K. Das, "Adsorption, kinetics and equilibrium studies on removal of Cr(VI) from aqueous solutions using different low-cost adsorbents," *Chem. Eng. J.*, vol. 137, no. 3, pp. 529–541, 2008.

[63] M. O. Maebana, S. B. Mishra, B. B. Mamba, and A. K. Mishra, "Study on the efficiency of ethylene vinyl acetate-fly ash composites for the uptake of phenols from synthetic waste water," *J. Appl. Polym. Sci.*, vol. 128, no. 3, pp. 2073–2080, 2013.

[64] Y. Liu and L. Shen, "From Langmuir kinetics to first- and second-order rate equations for adsorption," *Langmuir*, vol. 24, no. 20, pp. 11625–11630, 2008.